Dyes and Pigments 113 (2015) 96–101

Contents lists available at ScienceDirect

Dyes and Pigments

journal homepage: www.elsevier.com/locate/dyepig

Synthesis and characterization of the Bi-for-Ca substituted copper-based apatite pigments

M.A. Pogosova [a, *], D.I. Provotorov [a], A.A. Eliseev [a], M. Jansen [b], P.E. Kazin [a, 1]

[a] Department of Chemistry, Moscow State University, 119991 Moscow, Russian Federation
[b] Max Planck Institut für Festkörperforschung, Heisenbergstrasse 1, 70569 Stuttgart, Germany

ARTICLE INFO

Article history:
Received 16 May 2014
Received in revised form
22 July 2014
Accepted 28 July 2014
Available online 8 August 2014

Keywords:
Apatite
Pigment
Copper-doping
Crystal structure
Chromophore
Raman spectroscopy

ABSTRACT

Substitution of Bi for Ca in the red-violet pigment $Ca_{10}(PO_4)_6Cu_yO_2H_{2-y-\delta}$ has been studied in order to access possibilities to vary the color of the pigment. Synthesized compounds have been investigated by powder X-ray diffraction, diffuse reflectance (ultraviolet-visible-near infrared range) and Raman spectroscopy. Initial Bi-free samples contain Cu in the hexagonal channels, and a fraction of the Cu atoms constitutes recently discovered chromophore $[O–Cu^{III}–O]^-$-units. Bi^{3+} occupies Ca^{2+} position in the hexagonal channel walls and causes the reduction of the chromophore concentration. A small fraction of Cu^{2+} substitutes Ca^{2+} and forms a new chromophore characterized by the main absorption band at 400 nm and the resonant Raman band at 593 cm^{-1}. Consequently, Bi-doping suppresses the initial red-violet color of the pigment while a yellow tint emerges. This may open an opportunity to develop new less-toxic yellow pigments.

1. Introduction

In spite of the well-established manufacturing of inorganic pigments with a huge diversity in color there is a need to make the pigments more environmentally friendly and substitute some toxic or expensive pigments especially in the yellow-orange-red color range [1].

A new prospective pigment series developed recently represents alkaline-earth-metal phosphates $M_{10}(PO_4)_6(Cu_xO_2H_{2-x-\delta})$ with an apatite structure containing Cu-ions in the hexagonal channels [2–9]. The first brightly colored blue-violet copper-doped strontium hydroxyapatite was synthesized in 2002 [3]. Further investigations showed that copper doping made the barium hydroxyapatite blue and the calcium hydroxyapatite red-violet [4–6]. In these compounds, Cu-atoms formally substitute hydrogen of the $[OH]^-$ groups and are located at the (0,0,0) position. Such an arrangement provides linear coordination of Cu by two oxygen atoms (Fig. 1). The atomic group containing Cu^+ is described as a monomer $[O–Cu–O]^{3-}$-ion or an oligomer $[O\text{-}Cu_n\text{-}O_{n+1}]^{(n+2)-}$ inside the hexagonal channel of the apatite-type structure [3-8]. The color arises on partial oxidation of Cu^+ in the channel. Quite recently it has been established that copper in such compounds behaves a non-trivial way: it exists in two oxidation states, +1 and +3; and the color is produced by a new chromophore moiety, linear $[O–Cu^{III}–O]^-$-ion, confined in the channel [7]. It is characterized by the main absorption band at 595, 565, and 537 nm in the diffuse reflectance spectra of the Ba, Sr, and Ca-apatite respectively [3–5]. Hence the decrease of cation size and increase of a site-field effect (cation field strength) provides a regular blue-shift of the band. One may consider that a smaller cation or a cation with higher charge would further shift the band so that red-violet color of Ca-apatite would move to red-orange-yellow range.

Recently we have reported the results of Y- and Li-doping of the Ca-apatite pigment [8,9]. The introduction of Y causes almost total disappearance of the initial color. Y^{3+} substitutes Ca^{2+} only in position M(2), these cations form the walls of the hexagonal channels (Fig. 1) [9]. The increased positive charge of the walls is assumed to destabilize higher oxidation state of intrachannel copper ions, which makes the formation of the chromophore $[O–Cu^{III}–O]^-$ improbable. In contrast to that the Li-doping maintains the intense color with its certain change to a deeper wine-red tint, probably due to the low positive charge of Li-ion [8].

Obviously further research on the chemical modification of the pigment is required to find the ways to vary its brightness and tint. In the current paper we consider results of the Bi-doping of such

* Corresponding author. Tel.: +7 (495) 939 34 40.
E-mail addresses: pogosova.m.a@yandex.ru (M.A. Pogosova), delphinloko@rambler.ru (D.I. Provotorov), eliseev@inorg.chem.msu.ru (A.A. Eliseev), M.Jansen@fkf.mpg.de (M. Jansen), kazin@inorg.chem.msu.ru (P.E. Kazin).
[1] Tel.: +7 (495) 939 34 40.

http://dx.doi.org/10.1016/j.dyepig.2014.07.038
0143-7208/

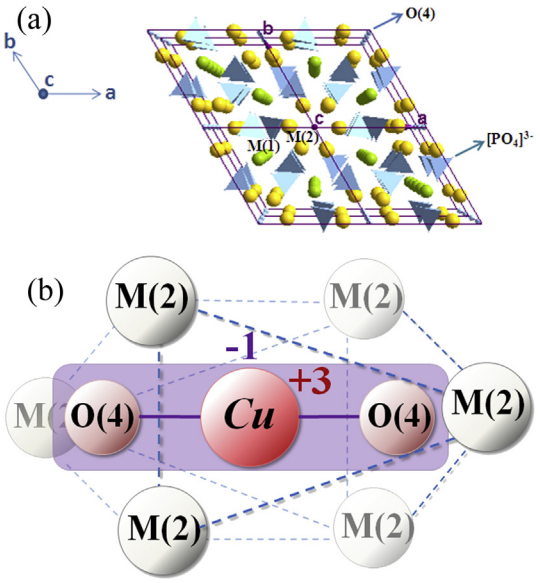

Fig. 1. Scheme of the apatite-type crystal structure (a.) and linear $[O–Cu^{III}–O]^-$ anion inside the hexagonal channel of the copper-doped hydroxyapatite (b.). M(1) represents the position of metal cations, which are surrounded by oxygen ions of the PO4 groups. M(2) represents the position of metal cations, which form the hexagonal channel's walls. Bismuth ions occupy only the M(2) position.

Ca-apatite pigments. In comparison with Y^{3+}, the cation Bi^{3+} has a bigger size (slightly exceeding that of Ca^{2+}) and forms the metal-oxygen bonds with higher covalent character. Therefore Bi^{3+} represent an interesting alternative dopant which may influence differently on the properties of the apatite pigments, at the same time providing high cation field strength required to keep the absorption band in the high-frequency region.

2. Experimental

Three types of the compounds based on calcium hydroxyapatite were prepared: bismuth-doped (Bi-for-Ca substituted), copper-doped (Cu-for-H substituted), bismuth-and-copper-doped, with general nominal composition $Ca_{10-x0}Bi_{x0}(PO_4)_6O_2H_{2-x0-y0-\delta}Cu_{y0}$, where x_0 = 0, 0.5, 1, 2 and y_0 = 0, 0.2, 0.6, further abbreviated as **B*x*$_0$C10*y*$_0$**. In addition, a cation-deficient sample $Ca_9Bi_{0.8}Cu_{0.2}(PO_4)_6O_2H_{1.4-\delta}$ was prepared and designated as **B0.8C2**. $CaCO_3$, $(NH_4)_2HPO_4$, Bi_2O_3 and CuO were mixed in appropriate stoichiometric amounts. A small excess of $CaCO_3$ (≈4%) was added to bismuth-free samples to suppress the formation of $Ca_3(PO_4)_2$. Samples were ground in an agate mortar and solid state synthesis was carried out according to the following scheme:

1. Heating in the muffle furnace for 2 h to 600 °C, holding for 1 h, then heating for 1 h to 800 °C, holding for 2 h. Cooling in the switched off furnace.
2. Heating for 1.5 h to 1000 °C (or 1150 °C for **B0C10*y*$_0$** series), holding for 5 h. Air quenching. This procedure was repeated 4 times.
3. Inserting into the preheated to 1000 °C (to 1150 °C for **B0C10*y*$_0$** series) muffle furnace and holding for 2 h. Air-quenching by pouring the powders on the aluminum foil cooled on ice.

Samples were ground in an agate mortar after each annealing. The air-quenching saves the color in contrast to free cooling in the switched-off furnace.

All powder XRD patterns were registered using a RIGAKU diffractometer (CuK_α radiation; angle range 2θ = 5–80°; step = 0.02°). Crystal structures of the synthesized materials were refined by the Rietveld method in space group $P6_3/m$ using the JANA 2006 software. Refined parameters were the following: unit cell dimensions, atomic positions (except hydrogen; O(4) was refined at the (0,0,*z*) split position) and thermal displacement factors, calcium–bismuth and copper occupancies at M(2) and (0,0,0) positions correspondingly. Using the occupancies, experimental *x* and *y* values were obtained for the composition $Ca_{10-x}Bi_x(PO_4)_6O_2H_{2-x-y-\delta}Cu_y$. Raman spectra were registered on a RENISHAW in Via Reflex (scanning range = 100–1500 cm^{-1}, λ = 514 nm). Diffuse reflection spectra were recorded on a Perkin Elmer Lambda 950 spectrometer (integrating sphere with SPECTRALON top-coating; the scanning step = 1 nm; output data was recalculated using Kubelka-Munk function; scanning range: from 350 to 1000 nm). Colorimetric measurements in CIE $L^*a^*b^*$ color space were provided using X-Rite Eye-One Pro monitor calibrator (scanning range = 400–800 nm; step = 10 nm; standard illuminant D_{50}) and reflex camera Olympus e-420 (5400K illuminant; ISO = 200; lightroom with length-width-depth = 35 cm − 25 cm − 32 cm) and the PhotoImpact 12 software. Correlation graphs on L^*, a^*, and b^* are presented in Appendices.

3. Results and discussion

3.1. Details of the crystal structure

The sample parameters under discussion are collected in Table 1. Scheme of the apatite lattice is shown in Fig. 1. All copper-doped samples are colored and all of the copper-free samples are white. The color of the copper-doped bismuth-free compounds is the same, as previously described for such pigments [4]. On the bismuth-doping the color of the copper-doped samples changes to lighter and softer tints. According to XRD analysis all obtained samples represent the apatite phase (Supplement, Fig. A1). Bismuth-free samples contain the $Ca(OH)_2$ and CaO admixtures. They may arise because of the small overstoichiometry of $CaCO_3$ in the initial mixture (see Experimental) which yielded CaO on annealing and $Ca(OH)_2$ on the subsequent sample exposure to air moisture. Bismuth-doped samples with the highest Cu-content contain the CuO admixture (less than 0.5%), indicating that not all of the copper has been incorporated in the crystal cell. In some samples, unidentified reflections are observed with intensities below 2%. In any case the content of the admixture phase (and intensity of the admixture reflections) did not exceed 3%.

Here we consider unit cell parameters, diameter of the hexagonal channel *d* (specified as double distance between the M(2) and (0,0,0.25) position), and occupancies of specific sites by Bi and Cu.

3.1.1. Bismuth-doped samples

Earlier it has been shown that upon the calcium by bismuth substitution in hydroxyapatite, the unit cell parameters increase [10], as it is expected considering a little bigger radius of Bi^{3+} in comparison with Ca^{2+} (1.03 and 1.00 Å respectively for coordination number 6) [11]. Furthermore, bismuth ions occupy only the M(2) position, and O(4) is located in the hexagonal channel at (0,0,0.25). As can be calculated from the data presented in Ref. [10] the distance M(2)-O(4) shrinks during the bismuth's doping. The considered distance is equal to half of the channel diameter *d*, therefore the latter also drops with the Bi^{3+} for Ca^{2+} substitution.

Our results confirm that on bismuth doping the cell parameters and unit cell volume *V* increases and *d* decreases (Fig. 2, Table 1); Bi^{3+} is located only at the M(2) position and its refined quantity *x* is close to the nominal value. The dependence between *V* and *x* is practically linear with the slope 4.486 $Å^3/x$. The channel diameter decreases approximately linearly with the slope −0.237 Å/*x*. The latter means that in spite of the bigger size of Bi^{3+} the M(2) atoms

Table 1
Characteristics of the samples $[Ca_4][Ca_{6-x}Bi_x](PO_4)_6Cu_yO_2H_{2-x-y-\delta}$. Color, *R*-factors, selected refined parameters of crystal structure (parameters of composition *x* and *y*, cell parameters *a* and *c*, cell volume *V*, hexagonal channel diameter *d*), and modeled parameters: $\Delta V = V - V_c$ and Cu-occupancy of M positions a_{ic}(Cu).

Sample	Color	R_{wp} (%)	R_{all} (%)	x[a]	y[a]	d, Å	a, Å	c, Å	V, Å^3	ΔV, Å^3[b]	a_{ic} (Cu)
B0C0	White	8.7	1.9	0	0	4.698 (2)	9.4205 (1)	6.8828 (1)	528.98 (1)	0	
B0C2	Rose	8.0	2.7	0	0.19	4.713 (2)	9.4255 (1)	6.8905 (1)	530.14 (1)	−0.16	
B0C6	Magenta	6.7	2.4	0	0.55	4.761 (3)	9.4356 (1)	6.9095 (1)	532.74 (1)	−0.04	
B0.5C6	Wine-brown	7.8	2.2	0.41	0.24	4.550 (3)	9.4335 (1)	6.9060 (1)	532.23 (2)	−0.50	0.007
B1C0	White	7.1	2.5	1.16	0	4.380 (3)	9.4410 (1)	6.9195 (1)	534.12 (2)	−0.03	
B1C2	Sand-yellow	6.0	2.4	0.98	0.12	4.419 (2)	9.4369 (1)	6.9196 (1)	533.67 (1)	−0.55	0.008
B1C6	Sand-beige	5.7	2.5	0.96	0.19	4.418 (3)	9.4364 (2)	6.9244 (1)	533.99 (2)	−0.62	0.009
B2C0	White	6.8	2.0	2.00	0	4.231 (2)	9.4564 (1)	6.9461 (1)	537.92 (1)	0.00	
B2C2	Gray	7.0	2.0	1.91	0.03	4.248 (3)	9.4491 (1)	6.9434 (1)	536.89 (1)	−0.90	0.013
B2C6	Dark-gray	7.4	2.9	1.89	0.01	4.237 (3)	9.4458 (1)	6.9429 (1)	536.47 (1)	−1.15	0.017
B0.8C2	Light-beige	7.0	2.7	0.93	0.17	4.451 (3)	9.4358 (1)	6.9128 (1)	533.02 (1)	−1.56	0.023

[a] Standard deviations are not more than 0.01.
[b] Standard deviations are not more than 0.05.

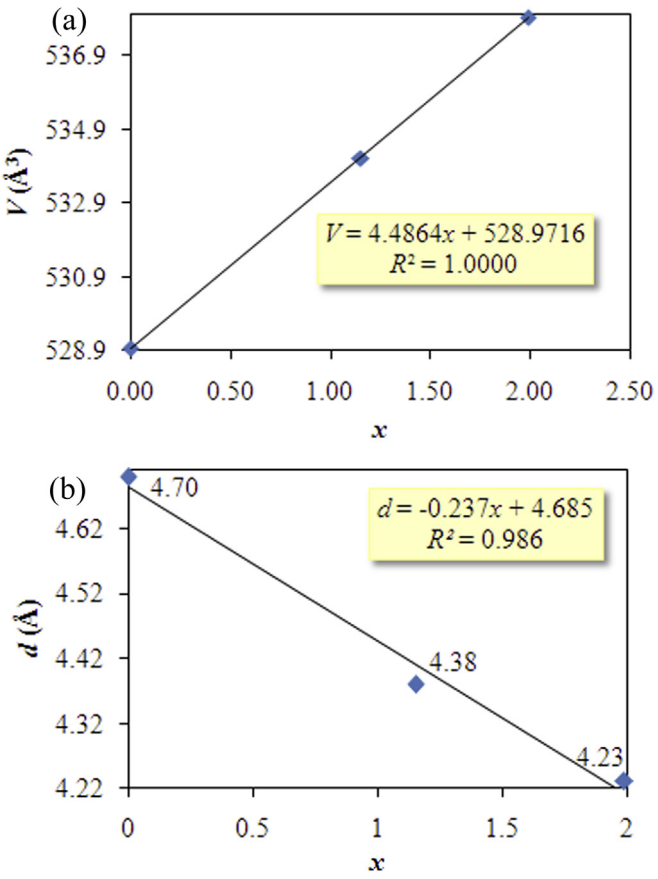

Fig. 2. Dependence of the unit cell volume *V* (a) and the hexagonal channel diameter *d* (b) on the content of bismuth *x* for $Ca_{10-x}Bi_x(PO_4)_6O_2H_{2-x}$ (samples **B0C0**, **B1C0**, **B2C0**).

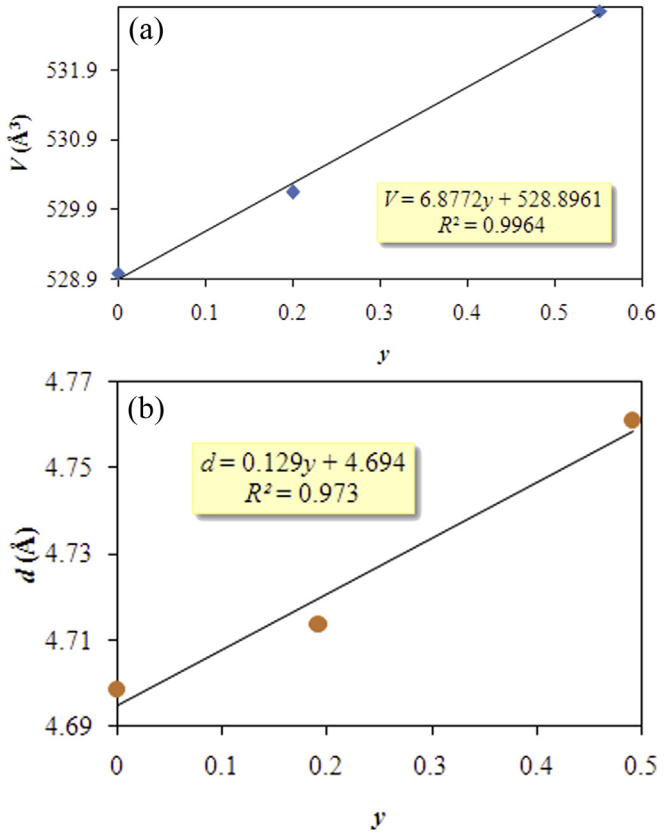

Fig. 3. Dependence of the unit cell volume *V* (a) and the hexagonal channel diameter *d* (b) on the content of copper *y* for $Ca_{10}(PO_4)_6O_2H_{2-y-\delta}Cu_y$ (samples **B0C0**, **B0C2**, **B0C6**).

approach each other and the M(2)-O(4) distance shortens. This effect can be explained considering two factors:

1). As it has been shown in Ref. [10], on the heterovalent Ca^{2+} by Bi^{3+} substitution, the proton of the OH^- group is removed and the higher charged O^{2-} anion is formed inside the hexagonal channel. Hence a stronger Coulomb attraction shortens the distance between M(2) and O^{2-} which makes the channel diameter decrease.
2). Due to higher charge and polarizability of Bi^{3+} and consequently more covalent nature of the $Bi^{3+} - O^{2-}$ interaction, the length of the local bond Bi(2) − O(4) may be shorter than the Ca(2)-O(4) bond length. At the same time the distances from the Bi atom to the O atoms of phosphate groups may increase so that the Bi^{3+} for Ca^{2+} substitution provides the cell volume to grow in accord with the expected bigger size of Bi^{3+}.

3.1.2. Copper-doped samples

In accordance with previous work [3–9], the introduction of copper expands the apatite crystal lattice and Cu is found in the hexagonal channels at position (0,0,0). Copper is determined in the channels in quantities *y* which are slightly lower than the nominal ones (see Table 1). The dependence between *V* and *y* is practically linear with the slope 6.877 Å^3/*y* (Fig. 3a).

According to the crystal structure data [3–9] it can be concluded that apatites with intrachannel copper ions have larger *d* than copper-free ones, apparently because the size of the copper ion is much bigger than the size of the hydrogen ion. In our case, *d* of the **B0C10y_0** series also grows with *y* with the approximate slope 0.129 Å/*y* (Fig. 3b).

3.1.3. Copper-and-bismuth-doped samples

The determined *x*–values are close to the nominal values, while *y*-values are considerably lower than nominal values, especially when the copper doping level is high (Table 1). For the series with maximum copper content, **Bx_0C6**, the apatite structure seems saturated with Cu-ions as the excessive copper concentrates in the CuO admixture phase (ca. 0.5%). In this series, *y* regularly decreases with the increase of the bismuth content, so that *y* is close to zero in **B2C6**. (see Table 1). Hence bismuth-ions prevent the introduction of copper-ions into the hexagonal channels.

This behavior could be linked to the competition between two processes taking place in the hexagonal channel: the copper for hydrogen substitution in the $[OH]^-$ ion, and the $[O]^{2-}$ for $[OH]^-$ substitution compensating heterovalent Bi^{3+} for Ca^{2+} substitution. At $x = 2$ the compound contains only $[O]^{2-}$ in the channels, and no Cu-ions can be introduced there. At $x = 1$ theoretical maximum of copper content *y* is equal to 1. An experimental maximum value of *y* is 0.19 only. Here one can consider that the copper atom is connected to two oxygen atoms, and if one of the oxygen atoms is coordinated to bismuth, the shift of the electron density to Bi^{3+} may destabilize a dioxocuprate-anion. Thus the Cu–O–Bi contacts seem improbable. Under this condition and $x = 1$, one expects that no copper ($y = 0$) can be introduced in the channel for the regular location of Bi(2) and Ca(2), and part of copper, $y = 0.5$, for the statistical distribution of Bi and Ca in M(2)-site. The experimental *y*-value lies between these limits.

In order to discuss changes in the *V* values in the bismuth-and-copper-doped samples one would assume that the impact of the bismuth and copper doping is additive, and using the linear dependences of *V* obtained in the previous sections one obtains Equation (1):

$$V_c(x, y) = V(0, 0) + 4.486x + 6.877y \quad (1)$$

where *V*(0,0) is the unit cell volume of **B0C0** ($Ca_{10}(PO_4)_6(OH)_2$).

The difference between experimental and calculated values are shown in Table 1. The experimental *V*-values are regularly smaller than the theoretically estimated ones. The difference grows with the nominal copper content. Taking into account that only a part of the added copper is located in the channels one may assume that the unit cell shrinkage is caused by a copper for calcium substitution, because the radius of copper-ion (both Cu^+ and Cu^{2+}) is smaller than that of Ca^{2+}. As it is seen from Table 1 for both series of the Bi-doped samples, $x_0 = 1$ and 2, the growth of copper content *y* corresponds to the increase of the channel diameter, as it was observed in Bi-free samples. Introduction of copper in M(2)-position may diminish *d*. On the other hand, the incorporation of bismuth in the M(2) position strongly decreases *d*. Taking into consideration this fact and the limited accuracy of the determination of *d*, it is not safe to judge using the *d*–value whether Cu enters the M(2)-site or not. Therefore we can only consider a probable general content of Cu in M(1) and M(2) sites jointly.

By plotting the linear dependence of the alkaline-earth hydroxyapatite cell volume *vs*. the cation (Ca^{2+}, Sr^{2+}, Ba^{2+}) volume and average cation volume for mixed alkaline-earth apatites (Fig. 4, corresponding data are from Refs. [3–7]) and extending it to the volume of Cu^{2+}-ion we have roughly estimated the Cu for Ca–Bi substitution degree in accord with equation:

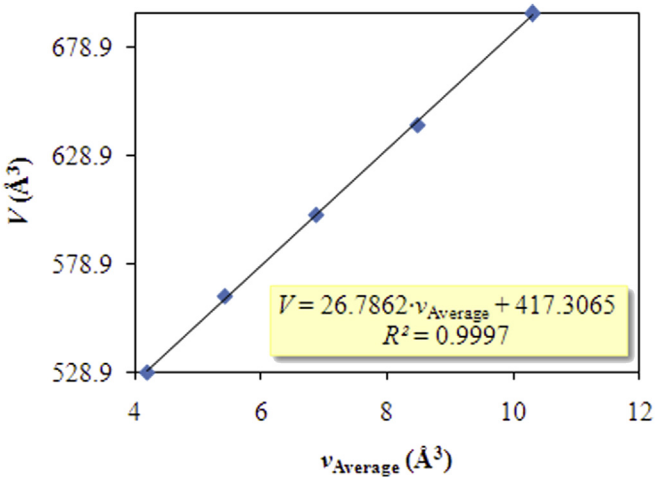

Fig. 4. The relationship between the unit cell volume *V* of $M_{10}(PO_4)_6(OH)_2$ and average volume $v_{Average}$ of alkaline-earth-metal cation M (for coordination number 6) [11].

$$a_{ic}(Cu) = (V_c - V)/(26.7862 \cdot (v_{(Ca2+)} - v_{(Cu2+)}) \quad (2)$$

The obtained values lie between 0.007 and 0.023 (see Table 1). Such a small substitution degree is hardly possible to estimate in the present structure refinement due to both, restricted accuracy of XRD and probable existence of vacancies sometimes found in M, e.g. in a lead phosphate [12]. The calculated copper occupancy shows a tendency to grow with the Bi-content. In the cation deficient **B0.8C2,** a_{ic}(Cu) reaches its maximum value, which is quite expected as the cation deficiency has to facilitate the substitution.

Therefore in copper-and-bismuth-doped apatites, copper-ions besides occupying the main intrachannel (0,0,0) position can to a small extent substitute Ca^{2+} in M-positions.

3.2. Raman spectroscopy

Raman spectra are shown in Fig. 5. All spectra contain bands of the $[PO_4]^{3-}$ group similar to those described in Refs. [10,13–19]. The band **Bi2** (Fig. 5) at 624 cm^{-1} observed in all bismuth-doped samples can be attributed to the Bi(2)-O(4) stretching mode, according to [10].

The spectra of the copper-doped samples contain the resonant band **Cu0** and its overtone at ~650 and ~1300 cm^{-1}, respectively. These bands have been observed in the spectra of the copper-doped alkaline-earth apatites and attributed to a new chromophore - linear $[O–Cu^{III}–O]^-$ anion [7]. In addition to this, one more resonant band, **Cu1** at 593 and its overtone at 1186 cm^{-1}, is observed in the spectra of copper-and-bismuth-doped samples only.

3.3. UV–VIS–NIR spectroscopy and colorimetry

Diffuse reflectance spectra of the **B0C2**, **B0.8C2**, **B1C2** and **B2C2** are presented in Fig. 6.

B0C10y_0 series. The spectra are typical of those described earlier for copper-doped calcium apatites [3–9]. The intense band **A** at 537 nm and weak band **B** at ~700 nm have been attributed to intrachannel copper-ions in an oxidation state above +1 [4–9]. Later such an oxidized copper moiety has been identified as a $[O–Cu^{III}–O]^-$-chromophore [7]. A middle-intensity band (shoulder) at 445 nm **C** and part of the absorption at 650–750 nm has been assigned to a small fraction of Cu^{2+} situated in other positions probably substituting Ca^{2+} [4–5]. It should be noted, that a fraction of Cu^{1+} located in the hexagonal channels imparts no color [3–5], as is usual for many compounds of Cu^+.

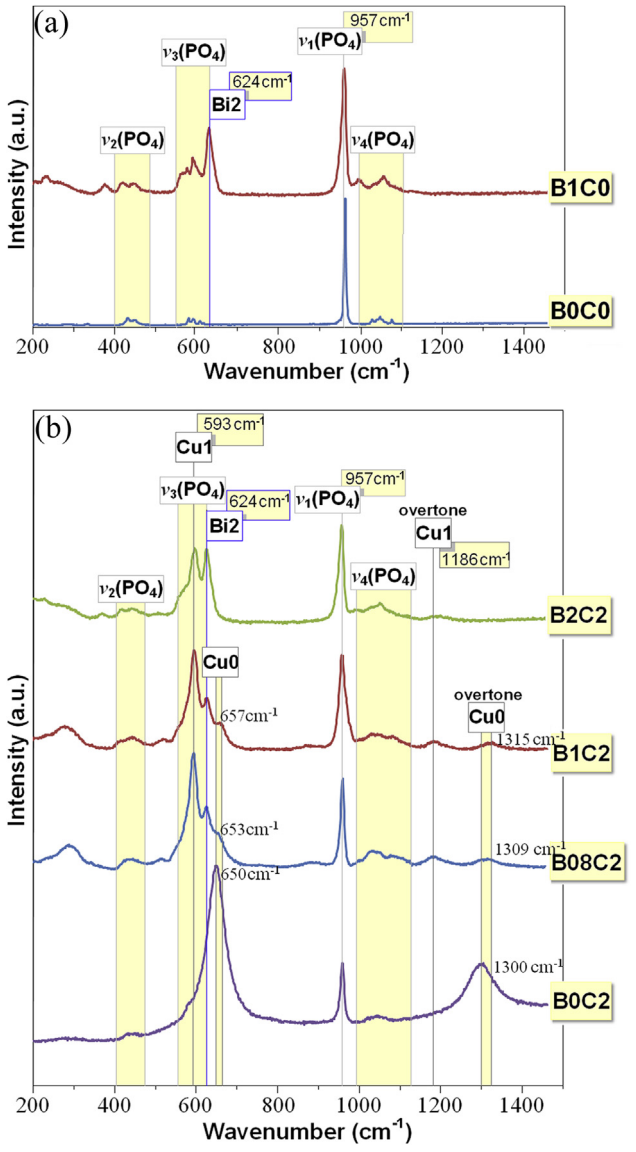

Fig. 5. Raman spectra of **B0C0** and **B1C0** (a), and **B0C2** – **B2C2** (b).

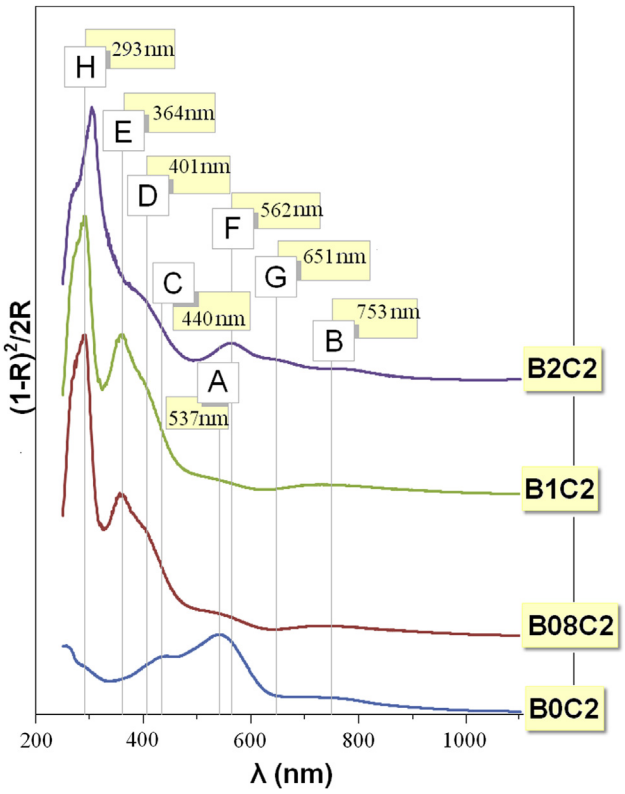

Fig. 6. Diffuse reflectance spectra of **B0C2**–**B2C2**. The absorption bands in the samples of bismuth-free pigment, B0C2 and B0C6 are labeled with **A**, **B** and **C**.

B1C10y_0 series and **B0.8C6**. Intensity of **A** strongly decreases. At 350 nm, a new strong band **E** arises with a shoulder **D** at ca. 400 nm instead of former **C** which disappears. Some increase in the absorption in the region of band **B** is also observed.

B2C10y_0 series. The spectra are characterized by the absence of **A**, **C**, **E** bands, increase of the **D** and **B** bands' intensity, and appearance of new bands, **F** and **G**.

The color changes of **Bx$_0$C2** samples are additionally described by colorimetry (Fig. 7; Table A2). It is seen that bismuth addition (**B08C2** and **B1C2**) causes the shift of the original color of **B0C2** to a yellow tint. Large amount of bismuth (**B2C2**) changes the color to a greyish tint. According to the correlation graphs (Fig. A3), results obtained by the Eye-One Pro monitor calibrator and the reflex camera Olympus e-420 are similar [20].

3.4. Relationships between the crystal structure and spectroscopic features

In the Raman spectra, the relative (to that of $\nu_1(PO_4)$) intensities of the main chromophore $[O–Cu^{III}–O]^-$ resonant band **Cu0** and its overtone strongly decrease with the increase of bismuth content *x*, and for **B2C2** the band totally disappears (see Fig. 5b.). Also, in the UV–VIS–NIR spectra the initial intensity of the corresponding absorption band **A** in **B0C2** drops multiply to **B1C2** so that only a shoulder of this band is left (see Fig. 6.). As soon as band **A** represents the chromophore $[O–Cu^{III}–O]^-$, we can conclude that bismuth for calcium substitution suppresses its formation. On going from **B0C2** to **B1C2**, the refined content of the intrachannel Cu, *y* decreases from 0.19 to 0.12. Taking into consideration that in this row, the Raman band **Cu0** intensity drops by a factor of ca. 7, a fraction of Cu^{3+} of all Cu in the channel should decrease ca. 5-fold. Hence substitution Bi^{3+} for Ca^{2+} suppresses the copper oxidation to Cu^{3+} in the channel. That is expected for such a heterovalent substitution since a lower positive charge of intrachannel cations is

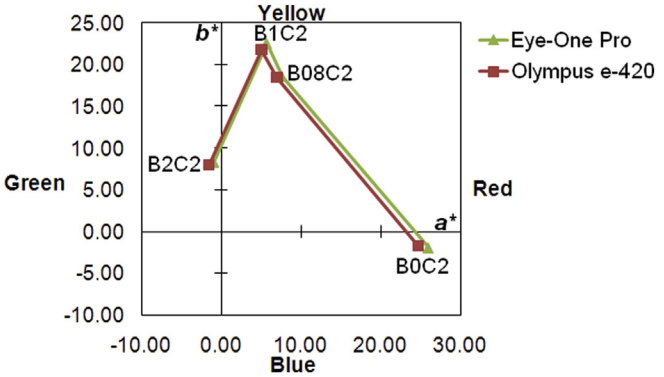

Fig. 7. Chromatic coordinates a^* and b^* for **BxC2** samples under standard illuminant D50 (Eye-One Pro) and 5400K (Olympus e-420).

required to keep electroneutrality. Bi-rich **B2C2** contains only 0.04 mol of intrachannel Cu. The dioxocuprate(III) chromophore is not observed in it, that limits its probable content (estimated from the Raman spectrum) to lower than 1% of the initial one in the Bi-free pigment.

With the Bi-doping a new kind of chromophore becomes pronounced. It is characterized by the near-UV band **D**. It is not also excluded that band **C** in the Bi-free sample **B0C2** belongs to the same chromophore and just blue-shifts to the **D**-position under Bi-doping. Simultaneously in the Raman spectra of Bi-doped samples, a new band at 593 cm^{-1}, **Cu1** with the overtone at 1186 cm^{-1} is becoming distinct. The presence of the overtone suggests its resonant character. The intensity of **D** and **Cu1** bands seems to correlate approaching their maximum values in the cation-deficient **B0.8C2**. Therefore this resonant band is reasonable to connect with the absorption **D** and consequently with the vibration of a new chromophore group. Band **D** persists also in **B2C6** in which *y* is close to zero within an estimation limit of ±0.01. Therefore the intrachannel copper is less probable to be the part of the new chromophore. As the crystal structure analysis evidences a partial substitution of Cu for Ca as was discussed above, the new chromophore may be considered as a Cu^{2+}-ion in this site. The resonant Raman band wavenumber is in the region of Cu–O stretching modes and most probably reflects the fully symmetric vibration of a CuO_n unit. Additional absorption near band **B**, which accompanies band **D**, may belong to the same chromophore center. For Cu^{2+}, an absorption in the **D**-region may arise due to charge–transfer transition and, in the **B**-region, due to d–d transitions [21]. The highest intensities of **D** and **Cu1** bands observed for **B0.8C2** also suggest the strongest Cu for Ca substitution, which is in accord with the largest value of the Cu occupancy calculated for this sample from the unit cell volume shrinkage.

Absorption band **F** in **B2C2** is close to initial band **A** in **B0C2**, but it does not originate from $[O–Cu^{III}–O]^-$ taking into account the absence of the corresponding resonant band in the Raman spectrum. Therefore band **F** and its satellite **G** cannot belong to Cu-ions of the $[O–Cu^{III}–O]^-$-anion. Absorption band **E** (in UV-region) being clearly visible only for **B1C2** and **B1C6** may relate to a weak additional feature at 515 cm^{-1} in their Raman spectra. Bands **F** + **G** and **E** may belong to non-identified moieties which most probably contain Cu-ions, as far as the Bi-only-doped samples do not reveal these features.

4. Conclusions

The doping of Cu-containing calcium hydroxyapatite pigment with Bi leads to substitution of Ca by Bi in the M(2)-position which is accompanied by the partial expulsion of Cu-ions out of hexagonal channels and hindering the oxidation of the remaining intrachannel Cu^{1+} to Cu^{3+} thereby suppressing the chromophore $[O–Cu^{III}–O]^-$-ion formation, characterized by the main adsorption band at 537 nm. The observed reduced values of crystal cell volume of the Bi-and-Cu-doped samples in comparison with the expected ones suggest that Cu-ions in a small amount enter the M-positions. Such samples reveal new UV–VIS–NIR absorption bands with the strongest one at ~400 nm, as well as a new resonant Raman band at 593 cm^{-1} tentatively assigned to the copper–oxygen stretching vibrations. As a result of all considered changes taking place with the Bi-doping, the former red-violet color of the pigment almost disappears while a yellow tint arises. The latter opens an opportunity to develop new less-toxic yellow pigments, taking into consideration lower toxicity and low content of Bi and Cu in the compound in comparison with lead and cadmium based pigments. Additional bands in visible region at ~560 and ~650 nm arisen in heavily Bi-doped samples may belong to a different chromophore moiety based on Cu-ions.

Acknowledgments

The work was partially supported by the RFBR project No 14-03-00643.

Appendix A. Supplementary data

Supplementary data related to this article can be found at http://dx.doi.org/10.1016/j.dyepig.2014.07.038.

References

[1] Jansen M, Letschert HP. Inorganic yellow-red pigments without toxic metals. Nature 2000;404:980–2.
[2] http://www.ferro.com (Performance pigments and colors. European markets. Pigment 28–5333).
[3] Kazin PE, Karpov AS, Jansen M, Nuss J, Tretyakov YD. Crystal structure and properties of strontium phosphate apatite with oxocuprate ions in hexagonal channels. Z Anorg Allg Chem 2003;629:344–52.
[4] Karpov AS, Nuss J, Jansen M, Kazin PE, Tretyakov YD. Synthesis, crystal structure and properties of calcium and barium hydroxyapatites containing copper ions in hexagonal channels. Solid State Sci 2003;5:1277–83.
[5] Kazin PE, Zykin MA, Tretyakov YD, Jansen M. Synthesis and properties of colored copper-containing apatites of composition $Ca_5(PO_4)_3Cu_YO_{Y+\delta}(OH)_{0.5-Y-\delta}X_{0.5}$ (X = OH, F, Cl). Russ J Inorg Chem 2008;53:362–6.
[6] Kazin PE, Zykin MA, Romashov AA, Tretyakov YD, Jansen M. Synthesis and properties of colored copper-containing alkaline-earth phosphates with an apatite structure. Russ J Inorg Chem 2010;55:145–9.
[7] Kazin PE, Zykin MA, Zubavichus YV, Magdysyuk OV, Dinnebier RE, Janzen M. Identification of the chromophore in the apatite pigment $[Sr_{10}(PO_4)_6(Cu_xOH_{1-x-y})_2]$: linear $OCuO^-$ featuring a resonance Raman effect, an extreme magnetic anisotropy, and slow spin relaxation. Chem Eur J 2014;20:165–78.
[8] Pogosova MA, Kazin PE, Tretyakov YD. Synthesis and characterisation of copper doped Ca–Li hydroxyapatite. Nucl Instr Methods Phys Res B 2012;284:33–5.
[9] Pogosova MA, Kazin PE, Tretyakov Yu D, Jansen M. Synthesis, structural features, and color of calcium–yttrium hydroxyapatite with copper ions in hexagonal channels. Russ J Inorg Chem 2013;58:381–6.
[10] Tmar Trabelsi I, Madani A, Mercier AM, Toumi M. Rietveld refinement and ionic conductivity of $Ca_{8.4}Bi_{1.6}(PO_4)_6O_{1.8}$. J Solid State Chem 2013;197:154–9.
[11] Lide R. Handbook of chemistry and physics. CRC press; 2001.
[12] White TJ, ZhiLi D. Structural derivation and crystal chemistry of apatites. Acta Cryst 2003;59:1–16.
[13] de Aza PN, Guitian F, Santos C. Vibrational properties of calcium phosphate compounds. 2. Comparison between hydroxyapatite and β-tricalcium phosphate. J Chem Mater 1997;9:916–22.
[14] Rosseeva EV, Buder J, Simon P, Schwarz U, Frank-Kamenetskaya OV, Kniep R. Synthesis, characterisation, and morphogenesis of carbonated fluorapatite-gelatine nanocomposites: a complex biomimetic approach toward the mineralisation of hard tissues. Chem Mater 2008;20:6003–13.
[15] Yu H, Zhang H, Wang X, Gu Z, Li X, Deng F. Local structure of hydroxy–peroxy apatite: a combined XRD, FT-IR, Raman, SEM, and solid-state NMR study. J Phys Chem Solids 2007;68:1863–71.
[16] O'Donnell MD, Fredholm Y, de Rouffignac A, Hill RG. Structural analysis of a series of strontium-substituted apatites. J Acta Biomater 2008;4:1455–64.
[17] Park JC, Huong PV, Rey-Lafon M, Grenier J-C, Wattiaux A, Pouchad M. Infra-red and Raman spectroscopic studies of superconducting electrochemically oxidized La2CuO4. J Phys C 1991;177:487–93.
[18] Wu MK, Loo BH. New synthesis route for cuprate oxide superconductors. J Phys C 1988;153-155:908–9.
[19] Ben-Dor L, Szerer MY, Blumberg G, Givan A, Borjesson L, Hong LV. Physical characterization and vibrational spectroscopy of Bi(Pb) cuprate 2212 ceramics prepared by sol-gel. J Phys C 1992;200:418–24.
[20] Apyari VV, Dmitrienko SG, Zolotov YA. Unusual application of common digital devices: potentialities of eye-one pro mini-spectrometer – a monitor calibrator for registration of surface plasmon resonance bands of silver and gold nanoparticles in solid matrices. J Sensors Actuators B: Chem 2013;188:1109–15.
[21] Solomon EI, Lever ABP. Inorganic electronic structure and spectroscopy. New York: John Wiley & Sons; 2006.